Superconducting Fluctuations Observed Far above T_c in the Isotropic Superconductor K_3C_{60}

Gregor Jotzu,[1,2,*] Guido Meier,[1] Alice Cantaluppi,[1] Andrea Cavalleri,[1,3] Daniele Pontiroli,[4]
Mauro Riccò,[4] Arzhang Ardavan,[3] and Moon-Sun Nam[3]

[1]*Max Planck Institute for the Structure and Dynamics of Matter, 22761 Hamburg, Germany*
[2]*The Hamburg Centre for Ultrafast Imaging, 22761 Hamburg, Germany*
[3]*Department of Physics, Clarendon Laboratory, University of Oxford, Oxford OX1 3PU, United Kingdom*
[4]*Dipartimento di Scienze Matematiche, Fisiche e Informatiche, Università degli Studi di Parma, Parma 43124, Italy*

(Received 20 September 2021; revised 21 December 2022; accepted 9 February 2023; published 17 April 2023)

Alkali-doped fullerides are strongly correlated organic superconductors that exhibit high transition temperatures, exceptionally large critical magnetic fields, and a number of other unusual properties. The proximity to a Mott insulating phase is thought to be a crucial ingredient of the underlying physics and may also affect precursors of superconductivity in the normal state above T_c. We report on the observation of a sizable magneto-thermoelectric (Nernst) effect in the normal state of K_3C_{60}, which displays the characteristics of superconducting fluctuations. This nonquasiparticle Nernst effect emerges from an ordinary quasiparticle background below a temperature of 80 K, far above $T_c = 20$ K. At the lowest fields and close to T_c, the scaling of the effect is captured by a model based on Gaussian fluctuations. The behavior at higher magnetic fields displays a symmetry between the magnetic length and the correlation length of the system. The temperature up to which we observe fluctuations is exceptionally high for a three-dimensional isotropic system, where fluctuation effects are expected to be suppressed.

DOI: 10.1103/PhysRevX.13.021008

Subject Areas: Condensed Matter Physics, Strongly Correlated Materials, Superconductivity

Recent work suggests that the exceptional properties of alkali-doped fulleride superconductors, A_3C_{60}, result from an unusual cooperation between electron-phonon and electron-electron coupling [1–4]. The former is primarily governed by a dynamical Jahn-Teller distortion of the C_{60} molecules, leading to an inverted Hund's coupling between electrons, while the latter contributes to a suppression of the effective bandwidth. With increasing lattice spacing, superconductivity in A_3C_{60} acquires a "domelike" T_c, eventually evolving into a Mott insulator with an antiferromagnetic ground state [5,6]. Unlike other high-temperature superconductors, however, A_3C_{60} features no anisotropy and displays the characteristics of an s-wave superconductor.

Additionally, A_3C_{60} seems to follow the Uemura relation [7,8], with a transition temperature T_c proportional to the superfluid density, suggesting that the loss of long-range phase coherence may be responsible for the disappearance of superconductivity at T_c. Yet, some uncertainty remains on this assignment because of the large spread of experimentally determined superfluid densities in A_3C_{60} [9,10].

In K_3C_{60} [see Fig. 1(a)], observables such as the specific heat and the pressure dependence of T_c suggest that the material may be well described by weak-coupling BCS theory [9,10], but discrepancies in the size and temperature dependence of the superconducting gap remain [11]. Very recent measurements in few-layer thin films of K_3C_{60} have reported the appearance of a pseudogap up to about twice T_c [12].

Finally, upon illumination with midinfrared laser pulses, optical properties compatible with superconductivity have been observed in K_3C_{60} at temperatures that exceed T_c by an order of magnitude [13–16], further underscoring a highly unusual normal state. Recent experiments have also provided suggestive magnetic anomalies when Rb_3C_{60} interacts with electromagnetic vacuum modes in an optical cavity [17]. One of the proposed mechanisms for these phenomena suggests that the effect of the light field consists in synchronizing preexisting, but phase-incoherent, Cooper pairs [15,18,19]. The magneto-thermoelectric effect known as the Nernst effect offers a powerful probe of the presence and nature of Cooper pairs above T_c [20].

*Corresponding author.
gregor.jotzu@mpsd.mpg.de

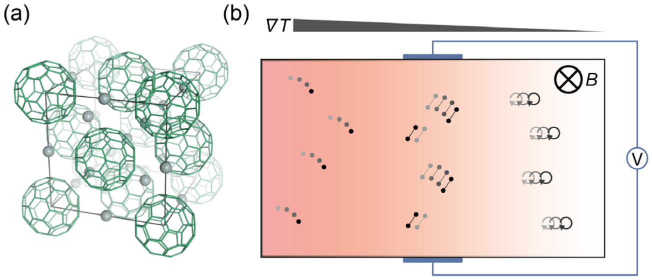

FIG. 1. Probing the Nernst effect in K_3C_{60}. (a) The fcc lattice structure of K_3C_{60}, with potassium atoms shown in gray and carbon buckyballs in green. (b) Schematic of the measurement configuration. A temperature gradient ∇T is applied orthogonally to the external magnetic field B. The voltage V is then measured orthogonally to both. Cartoons of various possible contributions to the Nernst signal, such as quasiparticles (left), short-lived Cooper pairs (center), and mobile vortices (right), are included.

The Nernst effect describes the appearance of an electric field, $E_y = -N\partial_x T$, transverse to an applied temperature gradient, $\partial_x T$, and to a magnetic field B_z pointing along the third spatial direction. The Nernst signal N is related to the conductivity and thermoelectric tensors, $\boldsymbol{\sigma}$ and $\boldsymbol{\alpha}$, via

$$N = \frac{\alpha_{xy}\sigma_{xx} - \alpha_{xx}\sigma_{xy}}{\sigma_{xx}^2 + \sigma_{xy}^2} \approx \frac{\alpha_{xy}}{\sigma_{xx}} - S\mu_{\mathrm{H}}B_z \tag{1}$$

for an isotropic system. Here, $\mu_{\mathrm{H}} = \sigma_{xy}/(\sigma_{xx}B_z)$ denotes the Hall mobility and $S = \alpha_{xx}/\sigma_{xx}$ the Seebeck coefficient. The approximate equality holds for small Hall angles and is an excellent approximation for the parameters used in this work.

For a metal, the effect can be seen as a combination of a flow of charges carrying entropy along a temperature gradient (the Seebeck effect) and the deflection of moving charges in the presence of a magnetic field (the Hall effect) [see Fig. 1(b)]. However, with exact particle-hole symmetry, the two terms in Eq. (1) would cancel exactly [21]. The overall sign and amplitude of the effect depend on the details of the quasiparticle band structure, to which the Nernst signal is very sensitive. The expected magnetic field dependence is linear. In the free-electron approximation, this signal is linear in temperature as well.

In a superconductor, a different contribution to the Nernst effect arises from the movement of superconducting vortices. When these mobile vortices carry entropy along the applied temperature gradient [see Fig. 1(b)], they also carry magnetic flux, which induces a voltage in the transverse direction [20]. This effect is characterized by a highly nonlinear dependence on B_z, perhaps owing to a competition between vortex density and vortex mobility.

If, at T_c, superconducting long-range order breaks down because of fluctuations of the phase of the order parameter while a finite Cooper pair amplitude remains, this vortex Nernst effect would be expected to survive at temperatures above T_c. However, even for a transition driven by a thermal breakdown of Cooper pairing, the thermal diffusion of short-lived Cooper pairs may also contribute to the Nernst signal above T_c [20,22,23].

In a number of materials, the superconducting contribution to the Nernst effect is much larger than its quasiparticle counterpart. Even precursors of superconductivity may exceed the quasiparticle background [20,23–28]. However, this cannot be assumed to be the case, in general [29,30]: The largest Nernst effect observed so far originates from quasiparticles in bismuth [20,31,32]. A careful analysis of the field and temperature dependence of the Nernst effect is therefore required to distinguish different contributions [27,33].

In general, the presence of such precursors of superconductivity is expected to be suppressed as the dimensionality of the system increases. Indeed, Nernst signals that could be related to superconducting precursors have been reported in layered materials, where the interlayer superconducting coherence length is short [24,25,27,33–39], and in thin-film samples with a thickness smaller than or comparable to the coherence length [23,26,28]. However, we are not aware of any previous observations in a microscopically isotropic and macroscopically three-dimensional system.

Interestingly, K_3C_{60} and Rb_3C_{60} were the first fully three-dimensional materials where slight deviations of the normal state conductivity in the immediate vicinity of T_c could be attributed to paraconductivity [40].

In the experiments reported in this paper, air-sensitive K_3C_{60} powders were compressed into pellets (see Appendix A) and incorporated into a circuit board printed on an FR4 substrate, which features low thermal conductivity. Embedded heaters and temperature sensors, as well as indium-coated contacts with contact resistances below 1 Ohm, were used to optimize these measurements (see Appendix B and Fig. 6). Four-probe resistance measurements (see Appendix C) were used to identify the superconducting transition, as shown in the inset of Fig. 2(a). In the zero field, we found $T_c(B=0) = 19.8$ K, in good agreement with previous reports and with magnetic measurements on the same batch of samples [9,10,14]. A Werthamer-Helfand-Hohenberg (WHH) theory [41] was used to extrapolate the zero-temperature upper critical field, $\mu_0 H_{c2}(0)$, from the field dependence of the resistive transition via $\mu_0 H_{c2}(0) = 0.69\mu_0 T_c(\partial H_{c2}/\partial T)|_{T_c}$, where μ_0 denotes the vacuum permeability. This yielded a value of about 39 T, corresponding to a zero-temperature coherence length of $\xi_0 = \sqrt{\Phi_0/2\pi\mu_0 H_{c2}(0)} = 2.9$ nm (here, Φ_0 is the magnetic flux quantum). This lies within the range of values extrapolated from other experiments [9,10] and closely matches the value recently determined using pulsed fields in a range exceeding H_{c2} [42]. Importantly, this value is also orders of magnitude smaller than the thickness of the sample or the powder grain size (see Appendix A), meaning that the description of the sample remains fully three dimensional throughout.

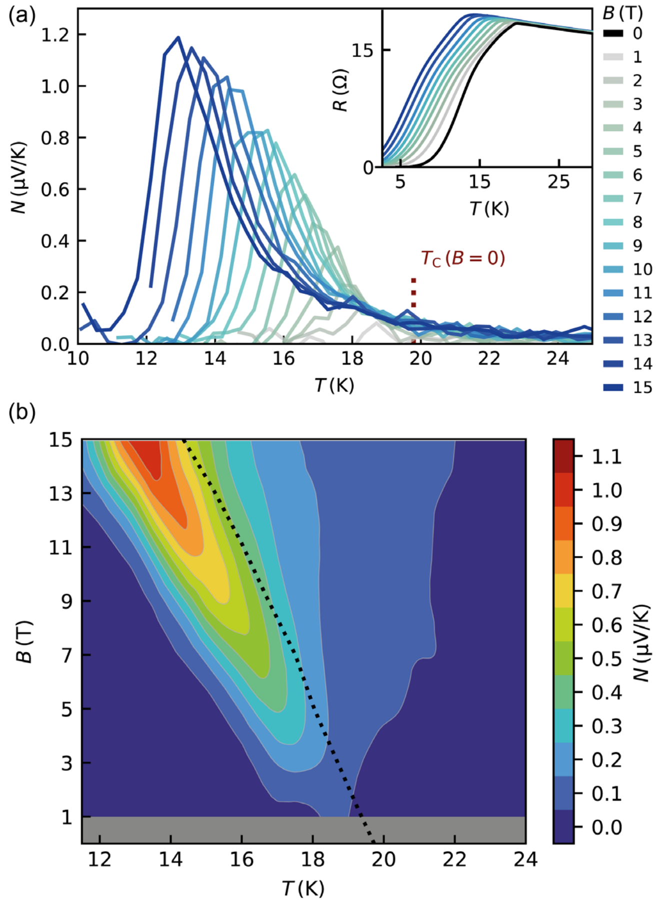

FIG. 2. Nernst signal in the superconducting regime. (a) Measured transverse thermoelectric effect N in the presence of magnetic fields ranging from 1 T (gray line) to 15 T (blue line), in steps of 1 T. The red dashed line shows the critical temperature in the zero field. Inset: sample resistance near the critical temperature, 0 T (black) to 15 T (blue) range. (b) Contour plot of N as a function of temperature and magnetic field. The black dotted line shows the resistive $T_c(B)$. A Gaussian convolution was used for smoothing, and in the low-T, low-B region, the data are sparse and interpolated. See Fig. 7(b) for raw data and the field-normalized N/B.

As expected, no Nernst signal (N) is observed for temperatures far below T_c, likely due to freezing of vortex motion. For higher temperatures, entering the temperature range where vortices become mobile, the signal is seen to increase [see Fig. 2(a)]. For a given magnetic field, the number of vortices in the system remains nearly constant (as all fields in our measurements are much larger than the lower critical field), but their mobility increases rapidly. Near T_c, the Nernst signal reduces again. A detailed quantitative understanding of this well-known phenomenon is still lacking—both the increasing vortex-vortex interactions that appear as vortex length scales increase and a change in the entropy per vortex are relevant [20,43]. However, very recent results suggest that an upper bound for this vortex Nernst effect may exist, and various superconductors spanning several orders of magnitude in critical fields and temperatures show signals that peak close to this bound [28]. Although the amplitude of N does not yet saturate at 15 T, the largest magnetic field achieved in our measurement, the value it seems to approach agrees with this upper bound—a quantitative discussion is found in Appendix D.

As a function of magnetic field, the Nernst signal in the superconducting phase is strongly nonlinear [see Fig. 7(a)] and peaks at a field $B_{\max}$ that reduces on approaching the critical temperature. This reduction fits very well to a linear function with a slope of $-2.27(3)$ T/K; see Fig. 4(a). It displays a zero-field intersect at $T = 19.5(1)$ K, close to the resistive critical temperature $T_c(B = 0) = 19.8$ K. Note that $B_{\max}$ has previously been shown to bear some similarity to a softening mode [20,29], and its vanishing value when approaching $T_c(0)$ suggests that the Nernst effect changes in nature when crossing T_c. Above T_c, this nonlinear magnetic field dependence persists and is compatible with the existence of a "ghost critical field"—more details are provided in Appendix E.

Above T_c, precursors of superconductivity may contribute to the Nernst signal, but quasiparticles can also play a role. The latter contribution is expected to scale linearly with magnetic field and temperature (at constant volume) for a simple metallic state [21].

We therefore used the temperature- and magnetic-field-normalized Nernst signal, $\mathcal{N} = N/BT = \nu/T$, in order to distinguish superconducting and quasiparticle contributions. Here, $\nu = N/B$ denotes the magnetic-field-normalized Nernst signal, generally referred to as the "Nernst coefficient."

In Fig. 3(a), $\mathcal{N}$ is shown to evolve smoothly across T_c, remaining positive and retaining a strong field dependence, as expected for a signal that is primarily caused by superconducting fluctuations. Strikingly, the inset in Fig. 3(a) shows that $\mathcal{N}$ displays near-universal behavior upon approaching the field-dependent critical temperature $T_c(B)$ [see also Figs. 4(b) and 7(d)]. Theoretical work on two-dimensional systems [44–46] predicted such behavior close to the phase transition given by $T_c(B)$, and our results suggest that this also holds in three dimensions.

At higher temperatures, we observed two characteristic features in the data [see Fig. 3(b)]. First, at $T_0(B) \approx 50$ K, the signal changed from positive to negative. The temperature of the zero crossing, $T_0(B)$, hence denotes the point where the superconducting and the quasiparticle contributions to the Nernst effect have the same magnitude. Note that $T_0(B)$ shows a field dependence similar to $T_c(B)$ [see Fig. 4(a)]. This suggests that the aforementioned observation, that the Nernst effect close to the phase transition tracks the field-dependent critical temperature $T_c(B)$, still remains visible at much higher temperatures.

Second, a minimum in $\mathcal{N}$ appears at $T_{\min}(B) \approx 80$ K, above which $\mathcal{N}$ shows a linear and positive slope. In order

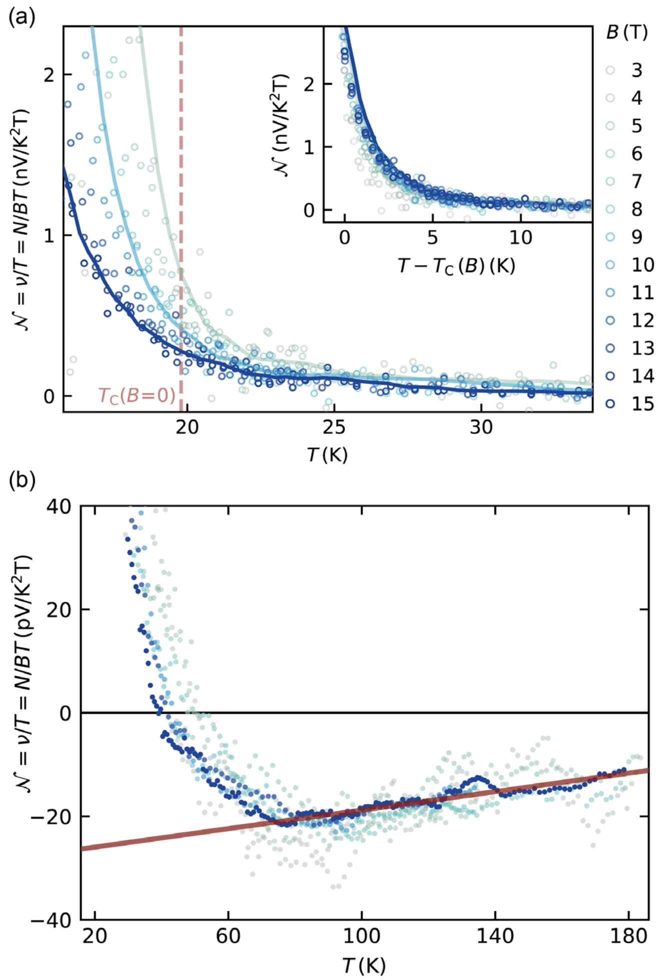

FIG. 3. Nernst effect above T_c. (a) Temperature and magnetic-field normalized Nernst signal $\mathcal{N}$ close to T_c (red dashed line). Open symbols show the raw data; lines are 10-point boxcar averages for 5 T, 10 T, and 15 T (gray to blue). Inset: same data rescaled with the field-dependent $T_c(B)$. (b) $\mathcal{N}$ at higher temperatures, after 10-point boxcar averaging (note the reduced y scale). The red curve corresponds to the quasiparticle contribution $-2.7\mu_{\mathrm{H}}S/T$.

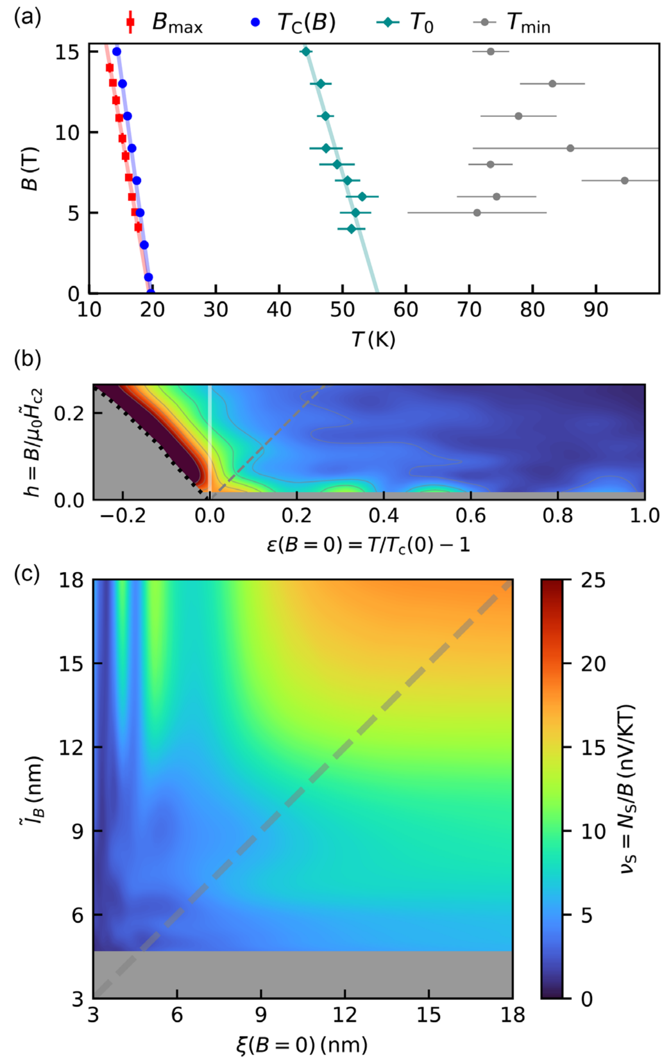

FIG. 4. Superconducting Nernst effect vs temperature and B field. (a) Characteristic quantities extracted from the Nernst signal: $B_{\max}$ denotes the fitted peak of $N(B)$ [see Fig. 2(b)]; T_0 and $T_{\min}$ are the zero crossing and minimum of $\mathcal{N}$, respectively; T_c denotes the resistive superconducting transition temperature. All lines are linear fits. Error bars indicate fit uncertainties. (b) Quasiparticle subtracted contribution to the Nernst coefficient ν_S as a function of dimensionless distance to the critical temperature ϵ and dimensionless field h. The black dotted line shows $T_c(B)$; the gray dashed line is $h = \epsilon$. (c) ν_S as a function of correlation length ξ and magnetic length $\tilde{l}_B$. The dashed line shows $\tilde{l}_B = \xi$.

to disentangle the superconducting contribution to $\mathcal{N}$, we first focus on the high-temperature limit, where the quasiparticle contribution should become dominant. We can compare the behavior of $\mathcal{N}$ in this regime to the expected signal in a single-band free-electron model of a metal, $|\mathcal{N}| \sim \mu_{\mathrm{H}}S/T$, with a prefactor of order unity [21]. This relationship implies that the Nernst effect is proportional to the ratio of the mobility and the Fermi energy in the metal, which was found to hold in a variety of materials, with $\mathcal{N}$ ranging from 1 $\mathrm{mV/K^2T}$ down to 1 $\mathrm{nV/K^2T}$ [20]. We use previously determined values for the T-linear S and μ_{H} [47,48], where the latter shows a linear dependence on temperature that has been shown to scale with the expansion of the lattice. As shown in Fig. 3(b), we find excellent agreement with our data above $T_{\min}$, using a quasiparticle contribution of $-2.7\mu_{\mathrm{H}}S/T$, and no discernible field dependence of $\mathcal{N}$. Given the complex band structure of K_3C_{60}, the agreement with such a simple scaling is remarkable. It extends its range of validity to values of $\mathcal{N}$ as low as 20 $\mathrm{pV/K^2T}$, which are 2 orders of magnitude smaller than those reported so far [20].

The rapid change in the slope of $\mathcal{N}$ around 80 K indicates a significant change in the electronic properties of the material. Such a change could, in principle, be caused by the appearance of charge-density wave order [49], and in a number of cuprate superconductors, a very similar feature was found to coincide closely with the pseudogap temperature T^* [27]. In K_3C_{60}, a transition to a frozen orientational disorder of the C_{60} molecules is known to occur but at a temperature very close to 200 K [50,51]. There are no observations pointing at the appearance of competing orders around 80 K, although it is worth noting that a certain deviation from linearity has been observed in the Seebeck effect, which has been attributed to electron-phonon coupling or precursors of superconductivity [47,52,53].

An effect related to the superconducting ground state seems much more likely, given that the magnetic field dependence of the Nernst effect in this regime tracks $T_c(B)$. In order to further explore the magnetic-field dependence of the effect, in Fig. 4(b) we plot the quasiparticle-subtracted Nernst coefficient $\nu_S = N_S/B = N/B + 2.7\mu_\mathrm{H}S$ as a function of the dimensionless temperature distance to the critical temperature $\epsilon = T/T_c(0) - 1$ and the dimensionless magnetic field $h = B/\mu_0\tilde{H}_{c2}$. Here, we use the Ginzburg-Landau critical field, which is based on the low-field extrapolation $\tilde{H}_{c2} = \mu_0 T_c(\partial H_{c2}/\partial T)|_{T_c}$. It differs from the WHH extrapolation by a factor of 0.69 (see Ref. [46] for details and for the expected universal behavior of the two-dimensional Nernst effect in these units). Close to the critical line (given by $h = -\epsilon$ for $h \ll 1$), the Nernst coefficient depends only on the dimensionless distance normal to the critical line. Above $T_c(0)$ (i.e., for $\epsilon > 0$), we observe an approximate symmetry with respect to the gray dashed line where $h = \epsilon$.

A physical explanation for this symmetry has been suggested in previous work on two-dimensional systems [44–46,54]. In the normal state, the superconducting contribution to the Nernst effect is determined by a single function of two length scales: the (temperature-dependent) Ginzburg-Landau correlation length $\xi = \xi_0/\sqrt{\epsilon}$ and the magnetic length $\tilde{l}_B = \sqrt{\hbar/(2eB)} = l_B/\sqrt{2}$, where e is the electron charge and $\hbar$ the reduced Planck constant [55]. In the low-field limit (where the magnetic length is large), the Nernst coefficient is determined only by the correlation length (see below), and it increases as the correlation length becomes longer when approaching T_c. However, at larger fields or very close to the critical point, the correlation length can become comparable to the magnetic length, which then limits the size of the Nernst coefficient.

In thin films of $Nb_{0.15}Si_{0.85}$, the Nernst coefficient is found to be approximately symmetric with respect to the line where the correlation length ξ equals the magnetic length $\tilde{l}_B$ [54]. In Fig. 4(c), we present the Nernst coefficient in K_3C_{60}, showing that this approximate symmetry can also be found in a three-dimensional system.

In the following, we consider two scenarios through which precursors of superconductivity could cause a Nernst effect far above T_c: a vortex-based Nernst signal surviving in a phase-fluctuating regime above T_c, or a signal caused by short-lived Cooper pairs.

For the latter scenario, a theory based on Gaussian fluctuations in a Ginzburg-Landau model [22] predicts a superconducting contribution to the transverse Peltier coefficient α_{xy}, which is proportional to the magnetic field and otherwise depends only on the correlation length ξ and fundamental constants. Together with the temperature-dependent conductivity of the sample, this allows for a prediction of the superconducting contribution to the Nernst coefficient, ν_SCG, given by

$$\nu_\mathrm{SCG} = \frac{N_\mathrm{SCG}}{B_z} = \frac{\alpha_{xy}^\mathrm{SCG}}{\sigma_{xx}B_z} = \frac{k_\mathrm{B}e^2}{12\pi\hbar^2}\frac{\xi}{\sigma_{xx}} \tag{2}$$

with

$$\xi = \frac{\xi_0}{\sqrt{\epsilon}} = \frac{\xi_0}{\sqrt{(T - T_c)/T_c}} \tag{3}$$

for a three-dimensional system. Here, k_B denotes the Boltzmann constant. The two-dimensional version of this theory is in good agreement with measurements on conventional [20,23,28] and some unconventional [29,33] superconductors. Its prediction of a field-independent Nernst coefficient applies to the low-field regime, where the correlation length ξ is short compared to the magnetic length l_B, and $T_c(B) \approx T_c(0)$. As it is a continuum theory, it may also become invalid once ξ becomes as short as the lattice spacing, and generally speaking, Ginzburg-Landau theory is only applicable in the vicinity of T_c.

In Fig. 5(a), we compare our measurements for fields up to 6 T to this theory by subtracting the fitted quasiparticle contribution determined above [red line in Fig. 3(b)] from the measured Nernst signal. See Appendix F and Fig. 9 for other possible subtraction schemes. We find that the data are overall well described by the simple $1/\sqrt{\epsilon}$ scaling predicted by the theory if we use a constant conductivity of 6 $(\mathrm{m}\Omega\,\mathrm{cm})^{-1}$.

The temperature dependence of the conductivity of the sample is small enough that it has a negligible effect in the regime where superconducting fluctuations are visible, both for the intrinsic conductivity and the effective conductivity of the compressed powder sample we study (see Appendix G and Figs. 9 and 10). Although we expect our measurement to be sensitive to the intrinsic conductivity rather than grain boundary effects [39,57], this value is still about 3 times larger than the conductivity of high-purity single crystals [9]. Interestingly, however, a very similar discrepancy was found in measurements of the paraconductivity [40], suggesting that the residual conductivity describing the transport properties of superconducting fluctuations may not be identical to the one extracted from direct measurements.

At higher temperatures, beyond the expected regime of validity of this model, deviations from the simple scaling occur, which might be captured by perturbative expansions [44,45], but further work would be needed to

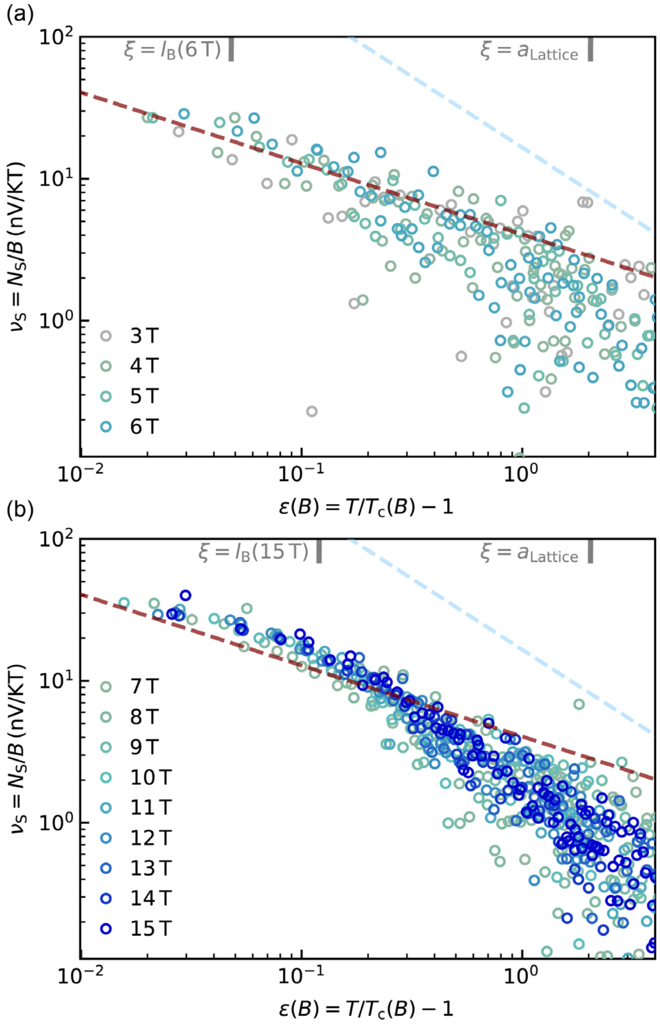

FIG. 5. Scaling of the superconducting Nernst coefficient above T_c. (a) Quasiparticle-subtracted contribution to the Nernst coefficient, $\nu_S = N_S/B = N/B + 2.7\mu_H S$, for magnetic fields between 3 T and 6 T. Color scale as in Fig. 1. The data are shown as a function of the distance to the field-dependent critical temperature at zero field. (b) Data for higher fields, up to 15 T. The dashed red line shows the expected low-field value from a model based on three-dimensional Gaussian fluctuations, which scales with $\epsilon^{-1/2}$. A constant conductivity of 6 $(\mathrm{m}\Omega\,\mathrm{cm})^{-1}$ is used (see text). The dashed blue line shows the equivalent signal for a two-dimensional system, which scales with ϵ^{-1}. The top axes indicate where the correlation length ξ becomes equal to the lattice spacing a_{Lattice} or to the magnetic length l_B at the highest field shown in the respective panel.

extend those theories to isotropic systems [58]. However, the data presented in Figs. 4 and 5 already show some of the qualitative features that would be expected within such a framework. In particular, the downturn at high temperatures, which was also observed in two-dimensional systems [20], may be an indication of the quantum nature of fluctuations [44]. Interestingly, at higher fields [see Fig. 5(b)], the behavior does not follow a single power law. This suggests that in a high field, the resistive $T_c(B)$ deviates from the thermodynamic critical point, which is a characteristic of unconventional superconductors [59].

Note that the theory presented above predicts a very different result for the Nernst coefficient in a (quasi) two-dimensional system [22]. There, $\alpha_{xy}^{2D}/B_z = \xi^2 k_B e^2/6\pi\hbar^2$, and a sheet resistance must be used to compute ν. The blue dotted line in Figs. 5(a) and 5(b) shows the expected signal under the assumption that a dimensional reduction of the system has taken place (see Appendix H), which was discussed in the context of alkali-doped fullerides [60]. Our results clearly deviate from this prediction, confirming the three-dimensional nature of the state we observe.

In order to gauge the plausibility of a phase-fluctuating scenario, we use the framework proposed by Emery and Kivelson [61] to estimate the temperature T_θ at which global phase coherence in the superconductor would be destroyed by thermal fluctuations—even if pairing were to survive up to a higher "mean field temperature" T_{MF}. Taking the most recent (and largest) value for the penetration depth in K_3C_{60}, $\lambda = 890$ nm [62], we find a temperature T_θ as low as 80 K. This is only 4 times larger than T_c, whereas for conventional superconductors, T_θ/T_{MF} can be on the order of 10^5. Additionally, by taking into account some degree of quantum fluctuations (as expected given the relative proximity of a Mott-insulating state), it is possible that the superconducting transition is somewhat suppressed below T_{MF}.

We are not aware of a quantitative prediction of the vortex Nernst signal above T_c in a three-dimensional system. Results in two dimensions [43] suggest an important role of the lattice geometry and therefore cannot simply be extrapolated to our system. As the difference between mean-field models and fully quantum-mechanical descriptions can become less pronounced in higher dimensions, good agreement of our data with a theory based on Gaussian fluctuations does not necessarily rule out agreement with a theory based on phase fluctuations.

Further theoretical work is therefore required for a quantitative distinction between these two theoretical scenarios. In particular, capturing the behavior at high temperatures and magnetic fields observed in our data could serve as an important benchmark for this comparison. On a qualitative level, the presence of an additional temperature scale (and hence an additional length scale) is expected to be visible in a phase-fluctuating scenario [63], but it does not seem to be observable in our data.

In the context of light-induced superconductivity in K_3C_{60}, our data provide an important input for any theoretical framework based on the synchronization of preexisting (stable or short-lived) but globally phase-incoherent Cooper pairs, which would also need to correctly describe the initial static state.

It would be highly interesting to extend our work to Rb_3C_{60} and especially $Rb_xCs_{3-x}C_{60}$, where quantum phase fluctuations caused by the proximity of the Mott-insulating state will be enhanced. For the latter family, a suppression in T_c upon approaching the quantum phase transition has been observed [5,6], but it could not be reproduced in an otherwise quantitatively successful theoretical model [1]. Studying the Nernst effect in this regime, which should be possible using the experimental framework presented here, would provide new insights concerning the nature of the superconducting transition in the fullerides, and of phase-incoherent superconductivity in general.

We thank Michele Buzzi, Dante Kennes, Daniel Podolsky, Dharmalingam Prabhakaran, and Maksym Serbyn for insightful discussions, and Boris Fiedler for superb technical assistance. This project was funded by the Cluster of Excellence "CUI: Advanced Imaging of Matter" (EXC 2056, Project No. 390715994) of the Deutsche Forschungsgemeinschaft (DFG, German Research Foundation), by the DFG Collaborative Research Center SFB 925 (Project No. 170620586), and by the Engineering and Physical Sciences Research Council (EPSRC, Grant code EP/P000479/1)

APPENDIX A: SAMPLE PREPARATION

The K_3C_{60} powder used in this work was prepared and characterized as previously reported in Refs. [13–15]. In brief, finely ground C_{60} powder and metallic potassium were placed in a vessel inside a Pyrex vial in stoichiometric amounts, evacuated to 10^{-6} mbar, and sealed. The two materials were heated at 523 K for 72 h and then at 623 K for 28 h, and kept separated to ensure that the C_{60} was only exposed to clean potassium vapor. After regrinding and pelletizing in an inert Ar atmosphere, the sample was annealed at 623 K for 5 days. Powder x-ray diffraction measurements confirmed the purity of K_3C_{60} and indicated a domain size between 100 nm and 400 nm. Optical microscopy measurements show grain sizes on the order of 10 μm. Magnetic susceptibility measurements yielded a T_c of 19.8 K [13]. For the Nernst effect and four-point resistivity measurements, the sample was handled inside an Ar glove box with less than 0.2 ppm O_2 and H_2O. It was placed inside an FR4 frame, which had been glued to the circuit board described below using thermally and electrically insulating, minimally outgassing glue (Epo-TeK 301-2FL-T); see Fig. 6. The powder was then compressed with an FR4 piston, hence creating a pellet of around 150-μm thickness, and sealed with the same glue. The resistance of the sample was monitored to ensure that no contamination occurred during the sealing process and the subsequent transfer to the cryostat.

APPENDIX B: NERNST EFFECT MEASUREMENT SETUP

We used a printed copper circuit board on an FR4 substrate (which featured a low thermal conductivity, about 0.1 W/Km at 10 K [64]), as shown in Fig. 6(b). Cernox temperature sensors were embedded in thermally conductive glue (Stycast 2850FT) in milled pockets on each side of the sample. They were used to monitor the temperature gradient across the sample, which was induced using a resistive heater. An additional Cernox sensor was attached to the bottom of the circuit board to monitor the base temperature. The circuit board was mounted to the cold finger of a cryostat using nonmagnetic (titanium) screws and spring washers, and PMMA spacers were used for additional thermal insulation. In the sample compartment, the copper contacts were coated with indium, yielding contact resistances below 1 Ohm. The transverse voltage was measured while slowly cooling the sample. Data for opposite magnetic fields [see Fig. 6(c)] were then subtracted to compute the Nernst signal.

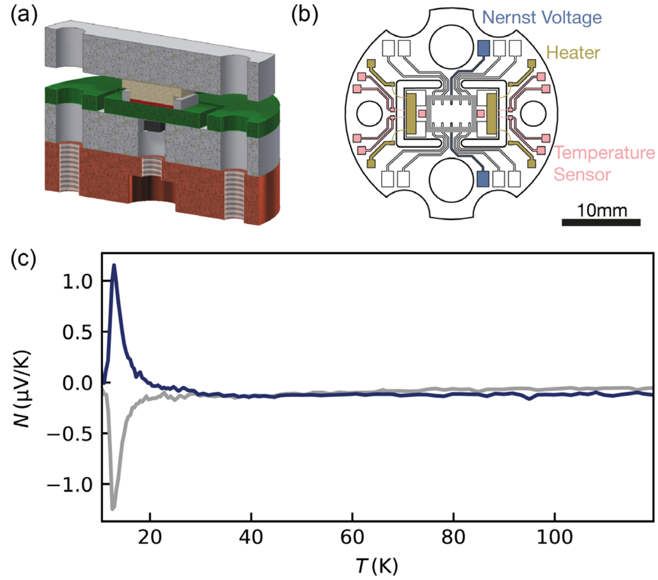

FIG. 6. Experimental setup. (a) Sample (red) pressed on top of a circuit board (green) using a PMMA piston (beige). The sample space is encapsulated using nonconductive epoxy glue. The base temperature is measured with a sensor (black) pressed against the bottom of the circuit board. The sample and circuit board are mounted on the cold finger of a cryostat (copper) using titanium screws (not shown), with spacers made of PMMA (gray). (b) Schematic of the circuit board. The sample compartment is indicated by a gray rectangle. A temperature sensor is placed on each side of the sample in a milled pocket, encapsulated by thermally conductive epoxy glue. Resistive heaters are placed on each side. The Nernst signal is measured with the indicated indium-coated contacts in the center of the sample compartment. The other contacts are used for four-point resistance measurements. (c) Transverse voltage at +15 T (blue) and −15 T (gray). For the data shown in the main text, the Nernst signal is evaluated as half of the difference between signals measured at opposite fields.

APPENDIX C: RESISTANCE MEASUREMENTS

The resistance of the sample was determined using a low-frequency lock-in measurement in a linear four-contact configuration, with contacts as shown in Fig. 6(b). Above T_c, the sample showed an increase in resistance upon cooling, as previously observed in granular K_3C_{60} samples [9,10]. In order to determine T_c, the point at which the resistance changes slope was used, which yielded a zero-field T_c consistent with magnetic susceptibility measurements on the same batch of sample. We verified that the width of the transition is not sensitive to reducing the probe current below the value of 2 μA that we used.

APPENDIX D: MAXIMUM VORTEX NERNST SIGNAL

Very recent results suggested that a universal upper bound for the vortex Nernst signal below T_c may exist [28]. By looking at Figs. 2(a) or 7(b), it is clear that for K_3C_{60} at 15 T, the signal has not reached its maximum possible value yet. However, a sublinear dependence of the peak in $N(T)$ as a function of magnetic field is already visible. Given the upper critical field of around 39 T, we can therefore estimate the largest value of $N(T, B)$ to be around 2 μV/K.

This value in itself is comparable to the values compiled by Rischau *et al.* [28]. The upper bound proposed in that work relates to the entropy per vortex per layer S_V, which can be determined from the Nernst signal N and the resistivity of the sample ρ via $S_V = \Phi_0 a_{\mathrm{Lattice}} N/\rho$, where $a_{\mathrm{Lattice}} = 1.42$ nm denotes the lattice spacing. Taking this ratio at the temperature and magnetic field corresponding to the peak in N, values for S_V very close to $k_B \ln 2 = 0.96 \times 10^{-23}$ J/K were found for a range of materials. As the resistivity of our samples is dominated by grain boundary effects, we use the intrinsic low-temperature normal resistivity of around $\rho_0 = 0.5$ mΩ cm [9] to estimate whether S may exceed $k_B \ln 2$. Taking a resistivity between ρ_0 and $\rho_0/3$ as a low guess for the resistivity at the peak of N (which lies below T_c, but at high fields, so that flux-flow resistance appears [28]) then yields values between 0.1×10^{-23} J/K and 0.4×10^{-23} J/K. This result is below, but reaches the same order of magnitude as, the upper bound identified in Ref. [28].

APPENDIX E: VISIBILITY OF THE GHOST CRITICAL FIELD

Previous theoretical and experimental work on the Nernst effect in two-dimensional and layered superconductors identified a "ghost critical field" at which the

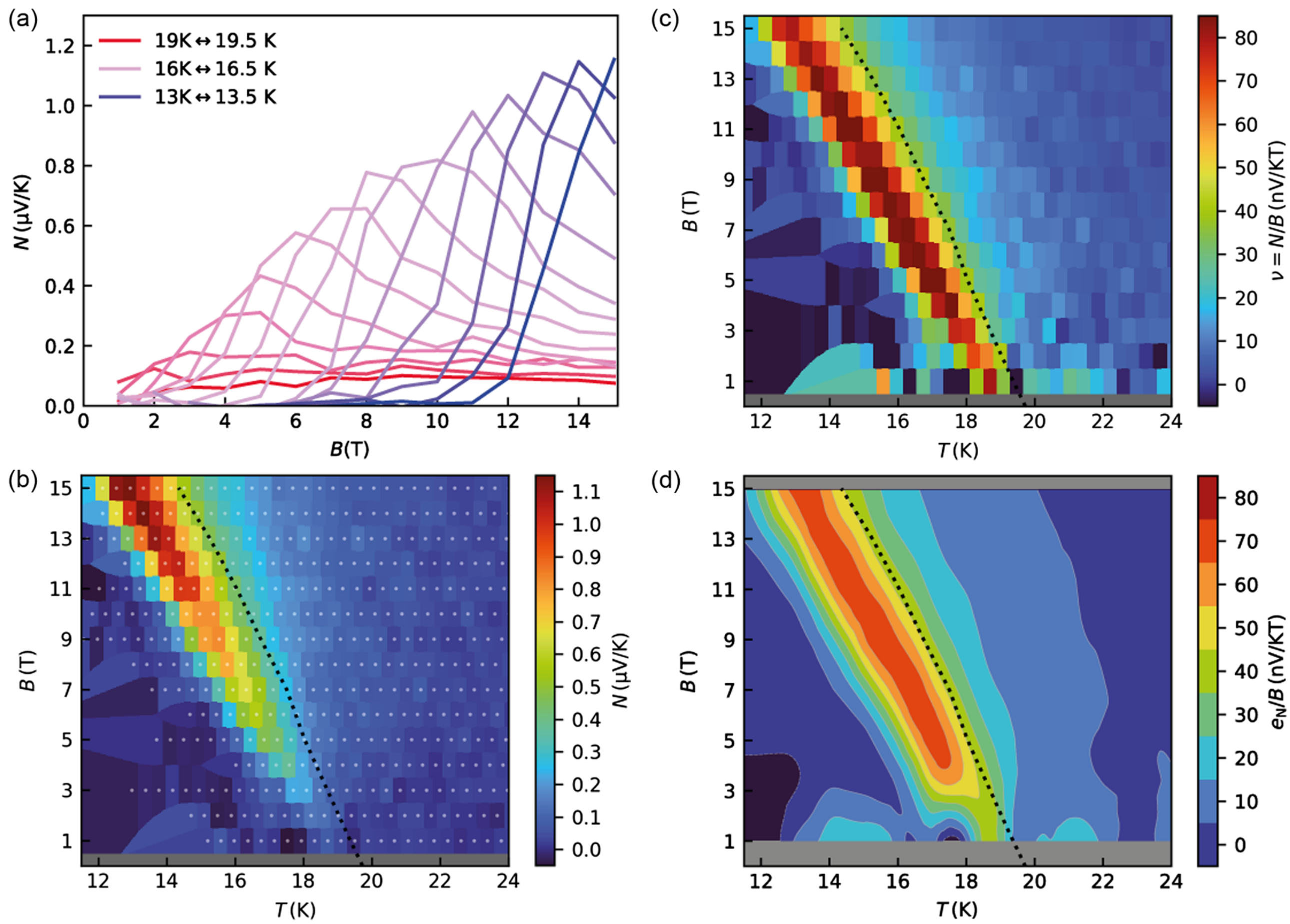

FIG. 7. *B-T* maps of the Nernst signal. (a) N as a function of magnetic field for different temperatures below $T_c(B)$. (b) Raw data of N as a function of temperature and magnetic field (see Fig. 2 for a smoothed contour map). Gray dots indicate the *B-T* values of each measurement; the data are interpolated to the nearest available point. The black dotted line shows $T_c(B)$. (c) Same as (b), but showing the field-normalized value N/B. (d) Smoothed contour plot of (c).

Nernst signal N (B) peaks, for a given temperature above T_c [26,29,33,46,54]. This happens when the magnetic length l_B becomes comparable to the correlation length $\xi(T)$. This ghost critical field is typically close to, but higher than, the "mirror field" given by the reflection around $T = T_c$ of the linear low-field limit of H_{c2}, i.e., given by $B_{\mathrm{Mirror}} = \mu_0(T - T_c)(\partial H_{c2}/\partial T)|_{T_c}$. Expressed in terms of the dimensionless quantities defined in the main text, this mirror field hence occurs where $h = t - 1$.

No exact analytical expression for the ghost field has been found so far, but numerical work reported in Ref. [46] has shown that, for a two-dimensional system, it can be approximated by the expression $h = 1.12t - 0.94$ as soon as the temperature is larger than about 1.07 T_c (i.e., about 21 K for our system). For temperatures closer to T_c, the ghost field rapidly approaches zero. Although the approximate solution found in 2D is unlikely to hold exactly in 3D, we can use it to estimate where the ghost critical field may appear in K_3C_{60}. We find that, for K_3C_{60}, the 2D expression for the ghost critical field reaches 15 T (the maximum field accessible in our experiment) at 21.3 K already. The mirror field reaches a value of 15 T at a temperature of 25 K (i.e., about 1.25 T_c). This means that our experiment is mostly carried out in a regime where the magnetic field acts as a linear probe of the intrinsic properties of the sample and does not impose an additional length scale for the thermodynamics of the Nernst effect.

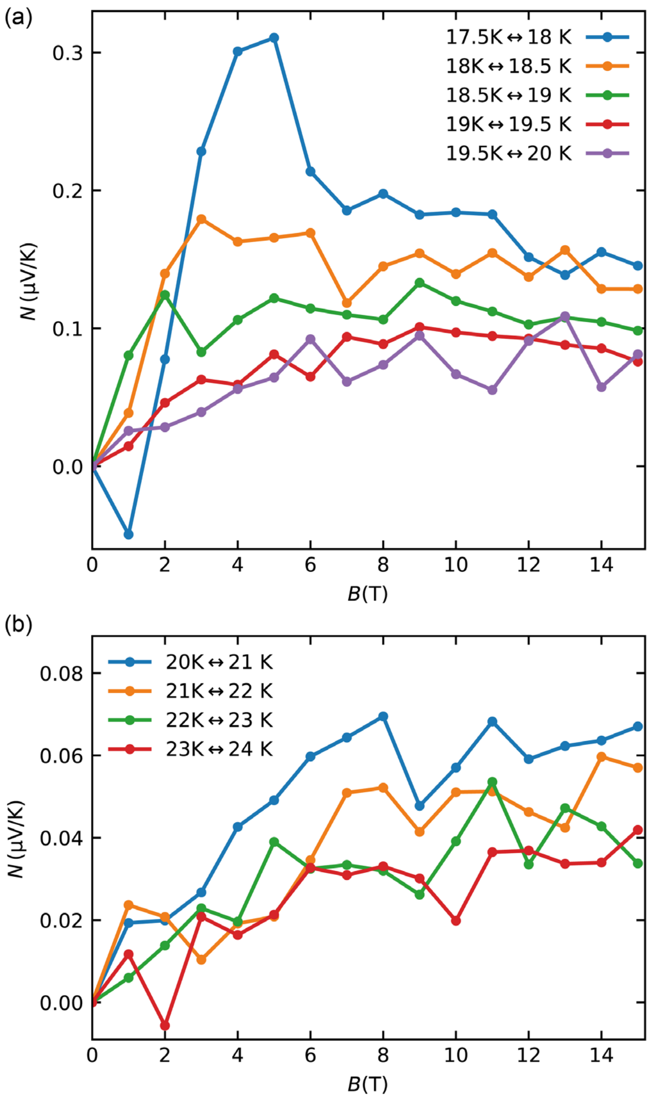

FIG. 8. Magnetic field dependence of the Nernst signal close to the critical temperature. (a) Quasiparticle-subtracted Nernst signal as a function of magnetic field for different temperatures just below T_c and just above T_c (b). Note the different vertical scales. A peak in N_s above $T_c(B)$ may indicate the presence of a ghost critical field (see text).

In the immediate vicinity of T_c, however, signatures of the ghost critical field may appear. Figure 8 shows the Nernst signal as a function of magnetic field, at different temperatures close to $T_c = 19.8$ K. Well below T_c, a sharp peak can be observed in the (quasiparticle-subtracted) Nernst signal (see also Fig. 7), which is the quantity shown as B_{max} in Fig. 3(c). Upon approaching T_c, the last range where a sharp peak can be identified is 17.5–18 K (see blue curve on the right). Above that range, $N_S(B)$ becomes more flat (similar to what was observed in NbSi [46]). Given the flatness of this feature, it is difficult to unequivocally determine the peak position; however, the data are compatible with a peak that moves towards even lower fields. For temperatures above T_c [Fig. 8(b)], our data are compatible with a peak in $N_S(B)$ that very rapidly moves towards higher fields. As outlined above, we expect that this peak may exceed 15 T at around 21 K, and indeed our data in the 20–21 K range already show that the peak has shifted to 8 T or higher, but sublinear behavior is still clearly visible.

APPENDIX F: SUBTRACTION OF THE QUASIPARTICLE SIGNAL

By comparing different subtraction schemes, we verify that the details of how the quasiparticle contribution to N is subtracted do not strongly affect the comparison to the Gaussian fluctuation model shown in Fig. 5: In Fig. 9(a), instead of subtracting the temperature-dependent quasiparticle function ($-2.7\mu_{\mathrm{H}}$S), we subtract its fixed value at 100 K. Here, the simple theoretical model seems to capture the data even at higher temperatures. In Fig. 9(b), we plot N without any quasiparticle subtraction. This leads to a deviation at high temperatures (as expected given that the signal changes sign there), but within the expected range of validity of the theoretical model, it still captures the data well. We have also verified that using a temperature-dependent value of the conductivity in Eq. (2) (where we have used the quadratic dependence found in Ref. [65] as a comparison) has a negligible effect in the relevant range.

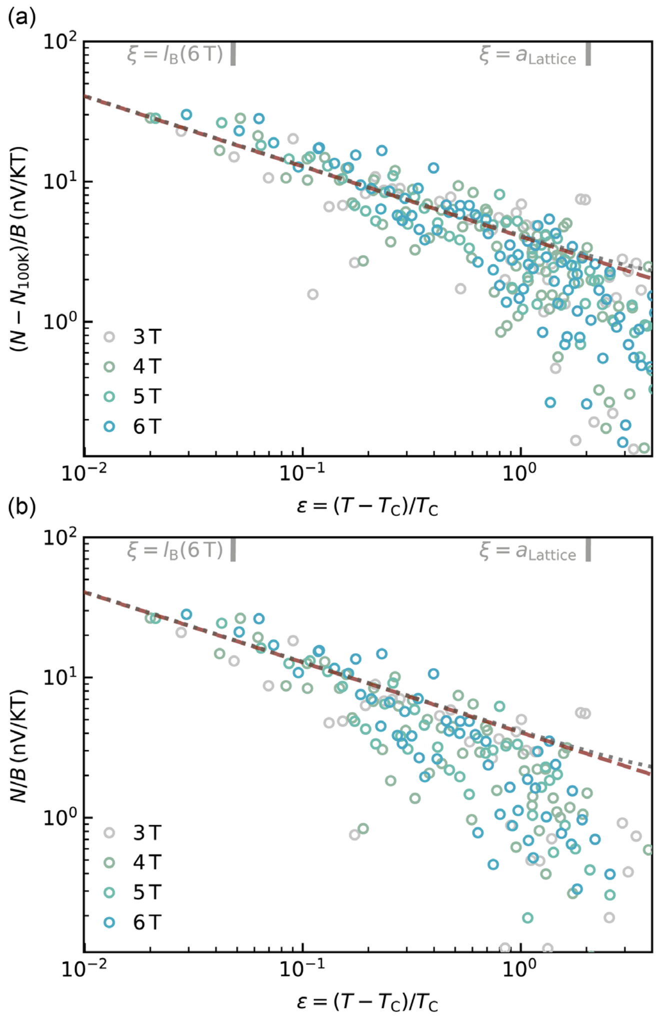

FIG. 9. Effect of subtracting the quasiparticle signal on the scaling analysis. (a) Same as Fig. 5(a), but subtracting the fixed value of N/B at 100 K instead of a temperature-dependent function. The gray dotted line shows the theoretical prediction of Eq. (2) but using a quadratic temperature dependence for the conductivity. (b) Nernst coefficient N/B without any subtraction of the quasiparticle contribution. Note that this results in some negative values for N at higher temperatures, which do not appear in this logarithmic plot.

APPENDIX G: RATIO OF NERNST COEFFICIENT AND RESISTIVITY

The theory for a Nernst effect caused by Gaussian superconducting fluctuations [22] predicts a result for the Nernst coefficient ν_{SCG} that depends only on the (temperature-dependent) correlation length ξ and the conductivity of the sample. As the conductivity of the sample is generally temperature dependent, this will affect the scaling of the Nernst coefficient with temperature. For K_3C_{60}, this effect is expected to be very small, as the change in the Nernst coefficient is much larger than the change of the conductivity. Figure 9 shows how taking into account the temperature dependence of the intrinsic conductivity would change the expected scaling (dotted gray line vs dashed dark red line). We additionally investigate the effect of temperature-dependent conductivity by dividing our measured Nernst coefficient $\nu_S = N_S/B$ by either the temperature-dependent intrinsic resistivity, ρ_I, based on measurements on single-crystal samples [9], or the measured temperature-dependent resistivity of our compressed powder sample, ρ_P (see Fig. 10). In both cases, we only find very small changes with respect to the scaling of the Nernst coefficient itself. Note that we do not expect the measured resistivity of the powder sample to be the correct quantity in order to determine the expected size of the Nernst effect: In a resistance measurement, current flows through grain boundaries, leading to a voltage drop that will provide the dominant contribution to the measured resistance. In a measurement of the Nernst signal, on the other hand, no current is flowing in the steady state (where the Nernst voltage is measured), meaning that the electrical resistance caused by grain boundaries does not contribute, and only the intrinsic resistivity of the sample determines the signal. See also Refs. [39,57] for theoretical and experimental work corroborating this statement.

APPENDIX H: COMPARISON TO TWO-DIMENSIONAL THEORY

In order to illustrate the distinct three-dimensional nature of our observations, there are two possible scenarios to take into account, in which the effect could become effectively two dimensional: First, one could consider the limit of a sample that is thin enough (in the direction of the magnetic field and transverse to the thermal gradient) that the correlation length ξ exceeds the thickness d. In that case, one would use the resistivity multiplied by the sample thickness as a sheet resistance. The expression for the Nernst coefficient for Gaussian superconducting fluctuations [Eq. (2)], $\nu_{\mathrm{SCG}} = (k_B e^2/12\pi\hbar^2)(\xi/\sigma_{xx})$, would become $(k_B e^2/6\pi\hbar^2)(\xi^2/\sigma_{xx} a)$; i.e., it would be multiplied by a (temperature-dependent) factor of $2\xi/d$. In the range explored in Fig. 5, this factor would range from 1×10^{-4} to 6×10^{-6}; i.e., the signal would be several orders of magnitude smaller than the signal predicted by the three-dimensional theory and observed in our data, in addition to having a different temperature dependence. Furthermore, as the Ginzburg-Landau correlation length remains below 10 nm even at the data closest to T_c and our sample has a thickness of around 150 μm (and even the smallest sample-related length scale, the size of the crystal domains, is between 100 nm and 400 nm), this scenario can be ruled out.

Second, a more realistic scenario would be that the sample might undergo spontaneous dimensional reduction in the applied magnetic field, as has been considered in the context of alkali-doped fullerides before [60]. In this case, the Lawrence-Doniach model could be used to describe such an effectively layered sample [see Eq. (14) in Ref. [22]]. The expected contribution to the Nernst coefficient would then be

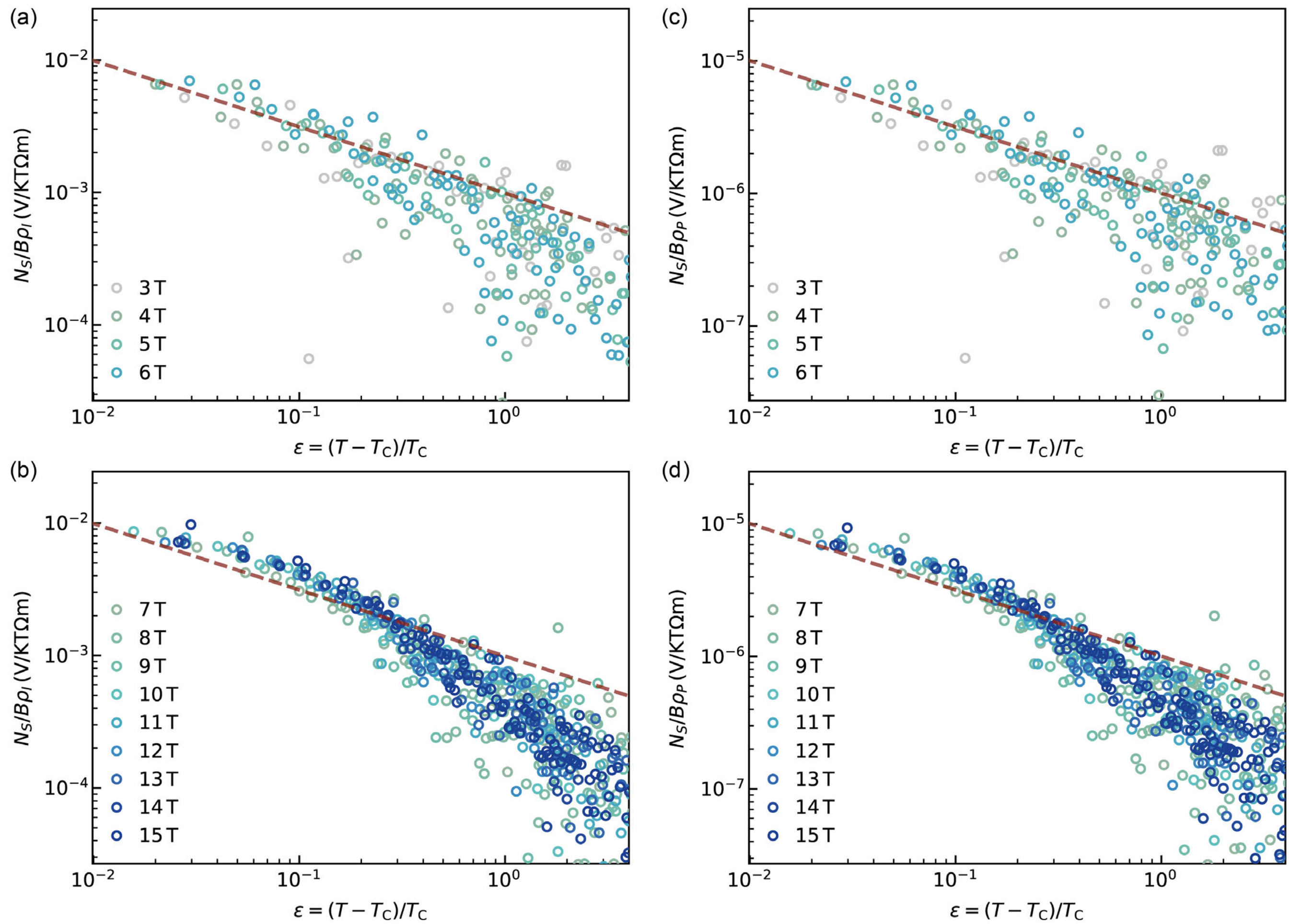

FIG. 10. Ratio of the Nernst signal and the resistivity. Same as Figs. 5(a) and 5(b), but divided by the intrinsic resistivity ρ_I of the sample (a,b) or the powder resistivity ρ_P (c,d).

$$\nu_{\mathrm{SCG}}^{\mathrm{LD}} = \frac{k_{\mathrm{B}} e^2}{6\pi\hbar^2} \frac{\xi_{xy}}{\sigma_{xx} a \sqrt{1 + (2\xi_z/a)^2}}, \tag{H1}$$

where $a = a_{\mathrm{Lattice}} = 1.42$ nm is the lattice spacing, and ξ_{xy} (ξ_z) denotes the correlation length transverse to (along) the B field. In the limit of a vanishing ξ_z (i.e., for completely decoupled layers), this essentially corresponds to taking the two-dimensional result for α_{xy} from Ref. [22] and using the resistivity multiplied by the lattice spacing as a sheet resistance. Compared to the 3D result for the Nernst coefficient ν, this corresponds to multiplying by a temperature-dependent coefficient of $2\xi/a$. We have included a plot of the expected signal in this scenario in Fig. 5 as a dashed blue line.

[1] Y. Nomura, S. Sakai, M. Capone, and R. Arita, *Exotic s-Wave Superconductivity in Alkali-Doped Fullerides*, J. Phys. Condens. Matter **28**, 153001 (2016).

[2] M. Capone, M. Fabrizio, C. Castellani, and E. Tosatti, *Strongly Correlated Superconductivity*, Science **296**, 2364 (2002).

[3] S. Chakravarty, M. P. Gelfand, and S. Kivelson, *Electronic Correlation Effects and Superconductivity in Doped Fullerenes*, Science **254**, 970 (1991).

[4] Phonon effects may not necessarily be required for an inverted Hund's coupling, see H.-C. Jiang and S. Kivelson, *Electronic Pair Binding and Hund's Rule Violations in Doped* C_{60}, Phys. Rev. B **93**, 165406 (2016).

[5] Y. Takabayashi, A. Y. Ganin, P. Jeglič, D. Arčon, T. Takano, Y. Iwasa, Y. Ohishi, M. Takata, N. Takeshita, K. Prassides, and M. J. Rosseinsky, *The Disorder-Free Non-BCS Superconductor* Cs_3C_{60} *Emerges from an Antiferromagnetic Insulator Parent State*, Science **323**, 1585 (2009).

[6] R. H. Zadik, Y. Takabayashi, G. Klupp, R. H. Colman, A. Y. Ganin, A. Potočnik, P. Jeglič, D. Arčon, P. Matus, K. Kamarás, Y. Kasahara, Y. Iwasa, A. N. Fitch, Y. Ohishi, G. Garbarino, K. Kato, M. J. Rosseinsky, and K. Prassides, *Optimized Unconventional Superconductivity in a Molecular Jahn-Teller Metal*, Sci. Adv. **1**, e1500059 (2015).

[7] Y. Uemura, A. Keren, L. Le, G. Luke, W. Wu, J. Tsai, K. Tanigaki, K. Holczer, S. Donovan, and R. Whetten, *System*

Dependence of the Magnetic-Field Penetration Depth in C_{60} *Superconductors*, Physica (Amsterdam) **235–240C**, 2501 (1994).

[8] Y. J. Uemura *et al.*, *Universal Correlations between* T_c *and* n_s/m^* *(Carrier Density over Effective Mass) in High-*T_c *Cuprate Superconductors*, Phys. Rev. Lett. **62**, 2317 (1989).

[9] O. Gunnarsson, *Alkali-Doped Fullerides: Narrow-Band Solids with Unusual Properties* (World Scientific, Singapore, 2004).

[10] K. M. Kadish and R. S. Ruoff, *Fullerenes: Chemistry, Physics, and Technology* (John Wiley & Sons, New York, 2000).

[11] C. M. Lieber and Z. Zhang, *Physical Properties of Metal-Doped Fullerene Superconductors*, Solid State Phys. **48**, 349 (1994).

[12] M.-Q. Ren, S. Han, S.-Z. Wang, J.-Q. Fan, C.-L. Song, X.-C. Ma, and Q.-K. Xue, *Direct Observation of Full-Gap Superconductivity and Pseudogap in Two-Dimensional Fullerides*, Phys. Rev. Lett. **124**, 187001 (2020).

[13] M. Mitrano, A. Cantaluppi, D. Nicoletti, S. Kaiser, A. Perucchi, S. Lupi, P. Di Pietro, D. Pontiroli, M. Riccò, S. R. Clark, D. Jaksch, and A. Cavalleri, *Possible Light-Induced Superconductivity in* K_3C_{60} *at High Temperature*, Nature (London) **530**, 461 (2016).

[14] A. Cantaluppi, M. Buzzi, G. Jotzu, D. Nicoletti, M. Mitrano, D. Pontiroli, M. Riccò, A. Perucchi, P. Di Pietro, and A. Cavalleri, *Pressure Tuning of Light-Induced Superconductivity in* K_3C_{60}, Nat. Phys. **14**, 837 (2018).

[15] M. Budden, T. Gebert, M. Buzzi, G. Jotzu, E. Wang, T. Matsuyama, G. Meier, Y. Laplace, D. Pontiroli, M. Riccò *et al.*, *Evidence for Metastable Photo-induced Superconductivity in* K_3C_{60}, Nat. Phys. **17**, 611 (2021).

[16] M. Buzzi, G. Jotzu, A. Cavalleri, J. I. Cirac, E. A. Demler, B. I. Halperin, M. D. Lukin, T. Shi, Y. Wang, and D. Podolsky, *Higgs-Mediated Optical Amplification in a Non-equilibrium Superconductor*, Phys. Rev. X **11**, 011055 (2021).

[17] A. Thomas, E. Devaux, K. Nagarajan, T. Chervy, M. Seidel, D. Hagenmüller, S. Schütz, J. Schachenmayer, C. Genet, G. Pupillo, and T. W. Ebbesen, *Exploring Superconductivity under Strong Coupling with the Vacuum Electromagnetic Field*, arXiv:1911.01459.

[18] Y. J. Uemura, *Dynamic Superconductivity Responses in Photoexcited Optical Conductivity and Nernst Effect*, Phys. Rev. Mater. **3**, 104801 (2019).

[19] M. Buzzi, D. Nicoletti, S. Fava, G. Jotzu, K. Miyagawa, K. Kanoda, A. Henderson, T. Siegrist, J. A. Schlueter, M. S. Nam, A. Ardavan, and A. Cavalleri, *Phase Diagram for Light-Induced Superconductivity in* κ-$(ET)_2$-X, Phys. Rev. Lett. **127**, 197002 (2021).

[20] K. Behnia and H. Aubin, *Nernst Effect in Metals and Superconductors: A Review of Concepts and Experiments*, Rep. Prog. Phys. **79**, 046502 (2016).

[21] K. Behnia, *The Nernst Effect and the Boundaries of the Fermi Liquid Picture*, J. Phys. Condens. Matter **21**, 113101 (2009).

[22] I. Ussishkin, S. L. Sondhi, and D. A. Huse, *Gaussian Superconducting Fluctuations, Thermal Transport, and the Nernst Effect*, Phys. Rev. Lett. **89**, 287001 (2002).

[23] A. Pourret, H. Aubin, J. Lesueur, C. A. Marrache-Kikuchi, L. Bergé, L. Dumoulin, and K. Behnia, *Observation of the Nernst Signal Generated by Fluctuating Cooper Pairs*, Nat. Phys. **2**, 683 (2006).

[24] Y. Wang, L. Li, and N. P. Ong, *Nernst Effect in High-*T_c *Superconductors*, Phys. Rev. B **73**, 024510 (2006).

[25] M.-S. Nam, A. Ardavan, S. J. Blundell, and J. A. Schlueter, *Fluctuating Superconductivity in Organic Molecular Metals Close to the Mott Transition*, Nature (London) **449**, 584 (2007).

[26] P. Spathis, H. Aubin, A. Pourret, and K. Behnia, *Nernst Effect in the Phase-Fluctuating Superconductor* InO_x, Europhys. Lett. **83**, 57005 (2008).

[27] O. Cyr-Choinière, R. Daou, F. Laliberté, C. Collignon, S. Badoux, D. LeBoeuf, J. Chang, B. J. Ramshaw, D. A. Bonn, W. N. Hardy, R. Liang, J.-Q. Yan, J.-G. Cheng, J.-S. Zhou, J. B. Goodenough, S. Pyon, T. Takayama, H. Takagi, N. Doiron-Leyraud, and L. Taillefer, *Pseudogap Temperature* T^* *of Cuprate Superconductors from the Nernst Effect*, Phys. Rev. B **97**, 064502 (2018).

[28] C. W. Rischau, Y. Li, B. Fauqué, H. Inoue, M. Kim, C. Bell, H. Y. Hwang, A. Kapitulnik, and K. Behnia, *Universal Bound to the Amplitude of the Vortex Nernst Signal in Superconductors*, Phys. Rev. Lett. **126**, 077001 (2021).

[29] F. F. Tafti, F. Laliberté, M. Dion, J. Gaudet, P. Fournier, and L. Taillefer, *Nernst Effect in the Electron-Doped Cuprate Superconductor* $Pr_{2-x}Ce_x$ CuO_4*: Superconducting Fluctuations, Upper Critical Field* H_{c2}*, and the Origin of the* T_c *Dome*, Phys. Rev. B **90**, 024519 (2014).

[30] T. Yamashita, Y. Shimoyama, Y. Haga, T. Matsuda, E. Yamamoto, Y. Onuki, H. Sumiyoshi, S. Fujimoto, A. Levchenko, T. Shibauchi *et al.*, *Colossal Thermomagnetic Response in the Exotic Superconductor* URu_2Si_2, Nat. Phys. **11**, 17 (2015).

[31] A. v. Ettingshausen and W. Nernst, *Ueber das Auftreten electromotorischer Kräfte in Metallplatten, welche von einem Wärmestrome durchflossen werden und sich im magnetischen Felde befinden*, Ann. Phys. (Berlin) **265**, 343 (1886).

[32] K. Behnia, M.-A. Méasson, and Y. Kopelevich, *Nernst Effect in Semimetals: The Effective Mass and the Figure of Merit*, Phys. Rev. Lett. **98**, 076603 (2007).

[33] J. Chang, N. Doiron-Leyraud, O. Cyr-Choiniére, G. Grissonnanche, F. Laliberté, E. Hassinger, J.-P. Reid, R. Daou, S. Pyon, T. Takayama, H. Takagi, and L. Taillefer, *Decrease of Upper Critical Field with Underdoping in Cuprate Superconductors*, Nat. Phys. **8**, 751 (2012).

[34] N. Ong, Y. Wang, S. Ono, Y. Ando, and S. Uchida, *Vorticity and the Nernst Effect in Cuprate Superconductors*, Ann. Phys. (Leipzig) **516**, 9 (2004).

[35] A. Kondrat, G. Behr, B. Büchner, and C. Hess, *Unusual Nernst Effect and Spin Density Wave Precursors in Superconducting* $LaFeAsO_{1-x}F_x$, Phys. Rev. B **83**, 092507 (2011).

[36] A. Pourret, L. Malone, A. B. Antunes, C. S. Yadav, P. L. Paulose, B. Fauqué, and K. Behnia, *Strong Correlation and Low Carrier Density in* $Fe_{1+y}Te_{0.6}Se_{0.4}$ *as Seen from Its Thermoelectric Response*, Phys. Rev. B **83**, 020504(R) (2011).

[37] M. S. Nam, C. Mézière, P. Batail, L. Zorina, S. Simonov, and A. Ardavan, *Superconducting Fluctuations in Organic Molecular Metals Enhanced by Mott Criticality*, Sci. Rep. **3**, 3390 (2013).
[38] S. Kasahara, T. Yamashita, A. Shi, R. Kobayashi, Y. Shimoyama, T. Watashige, K. Ishida, T. Terashima, T. Wolf, F. Hardy, C. Meingast, H. v. Löhneysen, A. Levchenko, T. Shibauchi, and Y. Matsuda, *Giant Superconducting Fluctuations in the Compensated Semimetal* FeSe *at the BCS–BEC Crossover*, Nat. Commun. **7**, 12843 (2016).
[39] S. D. Kang and G. J. Snyder, *Charge-Transport Model for Conducting Polymers*, Nat. Mater. **16**, 252 (2017).
[40] X.-D. Xiang, J. G. Hou, V. H. Crespi, A. Zettl, and M. L. Cohen, *Three-Dimensional Fluctuation Conductivity in Superconducting Single Crystal* K_3C_{60} *and* Rb_3C_{60}, Nature (London) **361**, 54 (1993).
[41] N. R. Werthamer, E. Helfand, and P. C. Hohenberg, *Temperature and Purity Dependence of the Superconducting Critical Field,* H_{c2}. *III. Electron Spin and Spin-Orbit Effects*, Phys. Rev. **147**, 295 (1966).
[42] Y. Kasahara, Y. Takeuchi, R. H. Zadik, Y. Takabayashi, R. H. Colman, R. D. McDonald, M. J. Rosseinsky, K. Prassides, and Y. Iwasa, *Upper Critical Field Reaches 90 Tesla Near the Mott Transition in Fulleride Superconductors*, Nat. Commun. **8**, 14467 (2017).
[43] D. Podolsky, S. Raghu, and A. Vishwanath, *Nernst Effect and Diamagnetism in Phase Fluctuating Superconductors*, Phys. Rev. Lett. **99**, 117004 (2007).
[44] K. Michaeli and A. M. Finkel'stein, *Fluctuations of the Superconducting Order Parameter as an Origin of the Nernst Effect*, Europhys. Lett. **86**, 27007 (2009).
[45] M. N. Serbyn, M. A. Skvortsov, A. A. Varlamov, and V. Galitski, *Giant Nernst Effect Due to Fluctuating Cooper Pairs in Superconductors*, Phys. Rev. Lett. **102**, 067001 (2009).
[46] A. Glatz, A. Pourret, and A. A. Varlamov, *Analysis of the Ghost and Mirror Fields in the Nernst Signal Induced by Superconducting Fluctuations*, Phys. Rev. B **102**, 174507 (2020).
[47] T. Inabe, H. Ogata, Y. Maruyama, Y. Achiba, S. Suzuki, K. Kikuchi, and I. Ikemoto, *Electronic Structure of Alkali Metal Doped* C_{60} *Derived from Thermoelectric Power Measurements*, Phys. Rev. Lett. **69**, 3797 (1992).
[48] L. Lu, V. H. Crespi, M. S. Fuhrer, A. Zettl, and M. L. Cohen, *Universal Form of Hall Coefficient in* K *and* Rb *Doped Single Crystal* C_{60}, Phys. Rev. Lett. **74**, 1637 (1995).
[49] R. Bel, K. Behnia, and H. Berger, *Ambipolar Nernst Effect in* $NbSe_2$, Phys. Rev. Lett. **91**, 066602 (2003).
[50] Y. Yoshinari, H. Alloul, G. Kriza, and K. Holczer, *Molecular Dynamics in* K_3C_{60}*: A* C^{13} *NMR Study*, Phys. Rev. Lett. **71**, 2413 (1993).
[51] A. Goldoni, L. Sangaletti, F. Parmagiani, S. L. Friedmann, Z.-X. Shen, M. Peloi, G. Comelli, and G. Paolucci, *Phase Transition, Molecular Motions, and Inequivalent Carbon Atoms in* K_3C_{60} *(111) Single-Phase Ordered Films*, Phys. Rev. B **59**, 16071 (1999).
[52] K. Sugihara, T. Inabe, Y. Maruyama, and Y. Achiba, *Thermoelectric Power of Alkali Doped* C_{60}, J. Phys. Soc. Jpn. **62**, 2757 (1993).
[53] D. T. Morelli, *Thermoelectric Power of Superconducting Fullerenes*, Phys. Rev. B **49**, 655 (1994).
[54] A. Pourret, H. Aubin, J. Lesueur, C. A. Marrache-Kikuchi, L. Bergé, L. Dumoulin, and K. Behnia, *Length Scale for the Superconducting Nernst Signal above* T_c *in* $Nb_{0.15}Si_{0.85}$, Phys. Rev. B **76**, 214504 (2007).
[55] Note that the definition of the magnetic length includes a factor of $1/\sqrt{2}$. This definition is chosen such that a comparison of the magnetic length and the correlation length is equivalent to a comparison of the dimensionless field and dimensionless amplitude. See the experimental work [54] and theoretical work [46,56] confirming this.
[56] W. J. Skocpol and M. Tinkham, *Fluctuations Near Superconducting Phase Transitions*, Rep. Prog. Phys. **38**, 1049 (1975).
[57] M. Soroka, K. Knížek, Z. Jirák, P. Levinský, M. Jarošová, J. Buršik, and J. Hejtmánek, *Anomalous Nernst Effect in the Ceramic and Thin Film Samples of* $La_{0.7}Sr_{0.3}CoO_3$ *Perovskite*, Phys. Rev. Mater. **5**, 035401 (2021).
[58] M. Serbyn (private communication).
[59] G. Blatter, M. V. Feigel'man, V. B. Geshkenbein, A. I. Larkin, and V. M. Vinokur, *Vortices in High-Temperature Superconductors*, Rev. Mod. Phys. **66**, 1125 (1994).
[60] S. Hoshino, P. Werner, and R. Arita, *Unconventional Orbital Ordering and Emergent Dimensional Reduction in Fulleride Superconductors*, Phys. Rev. B **99**, 235133 (2019).
[61] V. J. Emery and S. A. Kivelson, *Importance of Phase Fluctuations in Superconductors with Small Superfluid Density*, Nature (London) **374**, 434 (1995).
[62] V. Buntar, F. M. Sauerzopf, and H. W. Weber, *Lower Critical Fields of Alkali-Metal-Doped Fullerene Superconductors*, Phys. Rev. B **54**, R9651 (1996).
[63] I. Ussishkin and S. L. Sondhi, *On the Interpretation of the Nernst Effect Measurements in the Cuprates*, Int. J. Mod. Phys. B **18**, 3315 (2004).
[64] A. L. Woodcraft and A. Gray, *A Low Temperature Thermal Conductivity Database*, AIP Conf. Proc. **1185**, 681 (2009).
[65] O. Klein, G. Grüner, S.-M. Huang, J. B. Wiley, and R. B. Kaner, *Electrical Resistivity of* K_3C_{60}, Phys. Rev. B **46**, 11247 (1992).